


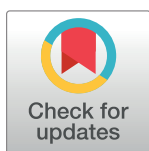
RESEARCH ARTICLE

Disruption of white matter connectivity in chronic obstructive pulmonary disease

Catherine A. Spilling¹ , Paul W. Jones², James W. Dodd³, Thomas R. Barrick^{1*}

1 Neuroscience Research Centre, Molecular and Clinical Sciences Research Institute, St George's University of London, Tooting, London, United Kingdom, **2** Institute of Infection and Immunity, St George's, University of London, Tooting, London, United Kingdom, **3** Academic Respiratory Unit, Second Floor, Learning and Research, Southmead Hospital, University of Bristol, Westbury-on-Trym, Bristol, United Kingdom

* tbarrick@sgul.ac.uk



Abstract

Background

Mild cognitive impairment is a common systemic manifestation of chronic obstructive pulmonary disease (COPD). However, its pathophysiological origins are not understood. Since, cognitive function relies on efficient communication between distributed cortical and subcortical regions, we investigated whether people with COPD have disruption in white matter connectivity.

Methods

Structural networks were constructed for 30 COPD patients (aged 54–84 years, 57% male, FEV₁ 52.5% pred.) and 23 controls (aged 51–81 years, 48% Male). Networks comprised 90 grey matter regions (nodes) interconnected by white matter fibre tracts traced using deterministic tractography (edges). Edges were weighted by the number of streamlines adjusted for a) streamline length and b) end-node volume. White matter connectivity was quantified using global and nodal graph metrics which characterised the networks connection density, connection strength, segregation, integration, nodal influence and *small-worldness*. Between-group differences in white matter connectivity and within-group associations with cognitive function and disease severity were tested.

Results

COPD patients' brain networks had significantly lower global connection strength ($p = 0.03$) and connection density ($p = 0.04$). There was a trend towards COPD patients having a reduction in nodal connection density and connection strength across the majority of network nodes but this only reached significance for connection density in the right superior temporal gyrus ($p = 0.02$) and did not survive correction for end-node volume. There were no other significant global or nodal network differences or within-group associations with disease severity or cognitive function.

OPEN ACCESS

Citation: Spilling CA, Jones PW, Dodd JW, Barrick TR (2019) Disruption of white matter connectivity in chronic obstructive pulmonary disease. PLoS ONE 14(10): e0223297. <https://doi.org/10.1371/journal.pone.0223297>

Editor: Niels Bergsland, University at Buffalo, UNITED STATES

Received: February 7, 2019

Accepted: September 19, 2019

Published: October 3, 2019

Copyright: © 2019 Spilling et al. This is an open access article distributed under the terms of the [Creative Commons Attribution License](https://creativecommons.org/licenses/by/4.0/), which permits unrestricted use, distribution, and reproduction in any medium, provided the original author and source are credited.

Data Availability Statement: All relevant data are within the manuscript and its Supporting Information files ([S1 File](#)).

Funding: The research was funded by St George's, University of London research funds, <https://www.sgul.ac.uk/>. PWJ received this funding. Since this was internal funding there is no grant number associated with this funding. The funders had no role in study design, data collection and analysis, decision to publish, or preparation of the manuscript.

Competing interests: I have read the journal's policy and the authors of this manuscript have the following competing interests: PWJ is employed as a Global Medical Expert for GlaxoSmithKline. JWD has received personal fees and travel support unrelated to the content of this manuscript from Chiesi, Boehringer Ingelheim & NAPP pharmaceutical. This does not alter our adherence to PLOS ONE policies on sharing data and materials. No other authors have any competing interests to declare.

Abbreviations: AUC, Area under the Curve; COPD, Chronic Obstructive Pulmonary Disease; DTI, Diffusion Tensor Images; DWI, Diffusion Weighted Images; FA, Fractional Anisotropy; FEV₁, Forced Expiratory Volume in one second; FSRP, Modified Framingham Stroke Risk Profile; FVC, Forced Vital Capacity; FEW, Family-Wise Error; HADS, Hospital Anxiety and Depression Scale; MNI, Montreal Neurological Institute; MMSE, Mini Mental State Examination; MR, Magnetic Resonance; MTPC, Multi-Threshold Permutation Correction; PCO₂, Partial Pressure of Carbon Dioxide; PO₂, Partial Pressure of Oxygen; SGRQ, St George's Respiratory Questionnaire; SVD, Cerebral Small Vessel Disease; τ , Network Threshold; t_{max} , Peak T-statistic; WMH(s), White Matter Hyperintensities of Presumed Vascular Origin.

Conclusion

COPD brain networks show evidence of damage compared to controls with a reduced number and strength of connections. This loss of connectivity was not sufficient to disrupt the overall efficiency of network organisation, suggesting that it has redundant capacity that makes it resilient to damage, which may explain why cognitive dysfunction is not severe. This might also explain why no direct relationships could be found with cognitive measures. Smoking and hypertension are known to have deleterious effects on the brain. These confounding effects could not be excluded.

Introduction

Mild cognitive impairment is a relatively common feature of a number of chronic diseases, including diabetes, kidney disease and rheumatoid arthritis [1–3]. Chronic obstructive pulmonary disease (COPD) is a chronic respiratory disease which is one of the leading causes of morbidity and mortality worldwide. It is associated with a number of extra-pulmonary co-morbid conditions, which occur more frequently in COPD than in smokers or never smokers, suggesting an intrinsic link to the disease [4]. One such co-morbidity is cognitive dysfunction, with estimates of its prevalence ranging from 10–61% [5]. Whilst the deficit is not universally very severe, its presence is associated with greater disability [6], poorer medication compliance [7] and an elevated risk of an exacerbation of their respiratory symptoms and mortality [6]. The pathophysiological origins of this cognitive dysfunction are not understood, but may involve structural and functional changes to brain anatomy secondary to cerebral small-vessel disease (SVD) [8–11]. Diffusion tensor imaging studies have reported a diffuse pattern of diffusion abnormalities in COPD suggestive of widespread deterioration of the tissue microstructure [10,12,13]. In SVD comparable diffusion abnormalities have been found to correlate more strongly with cognitive function and better predict cognitive decline and conversion to dementia [14] than conventional markers of SVD [15,16].

Cognitive function is reliant on efficient communication between networks of distributed brain regions interconnected by white matter fibre tracts [17,18]. This network complexity manifests as a hierarchical modular organisation (i.e. highly integrated sub-networks nested within larger networks) [19] featuring both global and nodal 'small-world' properties and an exponentially truncated power law degree-distribution indicative of the presence of a small number of heavily connected 'hub' brain regions [20]. It follows that pathology which disconnects white matter fibres or perturbs the network configuration, will be deleterious to function [17,18]. Indeed, it has been reported that the relationship between diffusion abnormalities and cognitive dysfunction in SVD is mediated by structural network disruption [21]. It is plausible that the same process is responsible for cognitive dysfunction in COPD.

The present study provides an exploratory cross-sectional patient-control investigation of large-scale structural networks in a well-defined cohort of stable patients with COPD. We hypothesised that patients with COPD would have impaired white matter connectivity relative to control subjects and that the magnitude of this network disruption would be related to lower cognitive function and greater disease severity.

Materials and methods

Subjects

31 stable COPD patients were recruited as part of a previous study [10]. Data from six of these patients were unavailable at the time of the original publication [10]. All participants were outpatients recruited from St George's University Hospital and Royal Brompton Hospital between 2010 and 2011, 17 of whom, had not been hospitalised within the preceding 12 months of data collection. The remaining 14 had previously been inpatients admitted to St. George's Hospital NHS Trust with a primary diagnosis of COPD exacerbation from whom data were obtained within 12 months of discharge. All participants were assessed whilst in a stable condition. Diffusion data was unavailable for one patient. Additionally, 26 non-COPD control subjects were recruited from the local community, three of whom were later excluded, two due to a scanner fault and one due to the presence of additional neuropathology (see [10] for a full list of exclusion criteria). This resulted in a cohort of 30 COPD patients and 23 controls. All participants provided written informed consent. This study was approved by Wandsworth and East Central London Research Ethics Committees (Ref: 10/H0721/16) and by St George's University of London, Joint Research Office (Ref: 090147).

Demographic and clinical characteristics of this cohort can be viewed in Table 1. To summarise, patients with COPD were well-matched for age and sex (aged 54–84 years, 57% male) compared to controls (aged 51–81 years, 48% Male). Patients with COPD met the Global Initiative for Chronic Obstructive Lung Disease (GOLD) classification [22] for moderate-severe airflow obstruction ($FEV_1 = 52.5 \pm 21.1\%$ pred., GOLD stage 3 (1), median (IQR)) and were not significantly hypoxaemic ($PO_2 = 9.9 \pm 2.5$ KPa) and were normocapnic ($PCO_2 = 5.0 \pm 0.7$ kPa). Patients with COPD had smoked for a significantly greater number of pack years and were significantly more anxious and depressed than controls (see Table 1). Only one COPD patient met the Mini Mental State Examination (MMSE) criteria for severe cognitive impairment, however, patients with COPD had significantly lower estimated pre-morbid IQ and lower cognitive function across all the cognitive domains assessed (see Table 1).

Statistical power

The sample size was informed by past empirical evidence and scientific reasoning. A sample size of $N = 55$ was chosen based on feasibility, economic grounds and previous research by other authors [11,23]. No formal power calculation was performed.

Cognitive and disease severity measures

Full details have been provided previously [10]. To summarise, post-bronchodilator spirometry, arterial blood gas analysis, a modified form of the Framingham Stroke Risk Profile (FSRP) [10,24], Charlson Co-morbidity Index [25] and a health status measure—the St George's Respiratory Questionnaire (SGRQ) [26] were administered to the patient group only. These measures were not collected for the controls as they were healthy individuals, therefore, we could not formally confirm that controls had normal lung function and blood gases. All subjects completed the Hospital Anxiety and Depression Scale (HADS) [27] and neuropsychological assessment, including the Mini Mental State Examination (MMSE), the Wechsler Test of Adult Reading (providing an estimate of pre-morbid IQ) and sub-scales taken from the Wechsler Adult Intelligence Scale–III, the Wechsler Memory Scale–III, the Delis-Kaplan Executive Function System, and the Rey-Complex Figure Test and Recognition Trial (see [10] for the specific subtests used). Composite scores were calculated, assessing the following cognitive domains: Executive Function (average of the Delis-Kaplan Executive Function System scaled

Table 1. Demographics.

	Controls	COPD	Statistic (df)	p
N	23	30		
Age	65.6 ± 7.4	67.2 ± 8.3	0.760 (51)	0.451 ¹
Males (%)	47.8	56.7	1.385	0.665 ²
Height (m)	1.7 ± 0.1	1.7 ± 0.1	-0.570 (45)	0.572 ¹
Body mass index (kg/m ²)	26.9 ± 4.7	26.6 ± 4.4	-0.266 (43)	0.792 ¹
Smoking (pack years)	0.0 (4.0)	53.5 (27.0)	682.5	<0.0001 ^{3****}
Cardiovascular risk (FSRP)	6.1 ± 3.2	7.2 ± 4.1	1.046 (51)	0.301 ¹
Exacerbations in last 12 months	-	1.0 (3.0)	-	-
SGRQ—total (health status)	-	53.7 ± 30.0	-	-
SGRQ—symptoms	-	62.9 ± 21.7	-	-
SGRQ—activity	-	73.2 (22.6)	-	-
SGRQ—impacts	-	41.8 ± 18.9	-	-
Co-morbidity Index	0 (0)	0 (1)	232.0	0.009 ^{3**}
HADS—anxiety	3.9 ± 2.8	7.4 ± 4.5	3.390 (44.4)	0.002 ^{1a**}
HADS—depression	1 (4)	5 (7)	3.061	0.002 ^{3**}
HADS—total	6.8 ± 5.0	11.8 ± 8.0	2.788 (49.4)	0.008 ^{1a**}
Cognitive Function				
Estimated pre-morbid IQ	110.0 (16.0)	103.0 (16.8)	-2.552	0.011 ^{3*}
Executive function	12.3 ± 2.6	9.4 ± 2.5	-4.096 (51)	<0.001 ^{1***}
Episodic memory	10.9 ± 3.1	9.3 ± 2.4	-2.147 (51)	0.037 ^{1*}
Processing speed	108.0 (18.0)	89.5 (24.8)	178.5	0.002 ^{3**}
Working memory	106.6 ± 15.5	94.2 ± 12.5	3.229 (51)	0.002 ^{1**}
MMSE	30.0 (1.0)	28.0 (2.0)	154.5	<0.001 ^{3***}
Lung Function				
FEV ₁ (% pred.)	-	52.5 ± 21.1	-	-
FVC (% pred.)	-	86.0 ± 32.1	-	-
FEV ₁ /FVC (%)	-	48.9 ± 15.8	-	-
GOLD Stage I (%)	-	10	-	-
GOLD Stage II (%)	-	31	-	-
GOLD Stage III (%)	-	35	-	-
GOLD Stage IV (%)	-	17	-	-
Normal FEV ₁ /FVC at assessment (%)	-	7	-	-
Arterial Blood Gases				
PO ₂ (kPa)	-	9.9 (2.5)	-	-
PCO ₂ (kPa)	-	5.0 (0.7)	-	-
pH	-	7.4 ± 0.0	-	-

Group comparison of demographic and clinical characteristics for the COPD patient group (aged 54–84 years, 57% male) and control group (aged 51–81 years, 48% Male). For Gaussian data,

¹independent t-tests, group means ± standard deviations, *t*-statistics, degrees of freedom (df) and *p*-values (*p*) are reported. For categorical data,

²chi-squared tests, group percentages, chi-square statistics and *p*-values (*p*) are reported. For non-Gaussian data,

³Mann-Whitney U tests, group medians (interquartile ranges), *U* statistics and exact probabilities (*p*) are reported.

^aCorrection for unequal variances.

Significant at **p*<0.05,

***p*<0.01,

****p*<0.001 and

*****p*<0.0001.

<https://doi.org/10.1371/journal.pone.0223297.t001>

scores), Episodic Memory (combined average of Wechsler Memory Scale–III and Rey-Complex Figure Test and Recognition Trial scaled scores), Processing Speed (Processing Speed Index from the Wechsler Adult Intelligence Scale–III) and Working Memory (Working Memory Index from the Wechsler Adult Intelligence Scale–III) [10].

Image acquisition and pre-processing

Magnetic resonance (MR) images were obtained for all subjects, using a 3-Tesla Philips Achieva dual TX scanner equipped with a 32-channel head coil and gradients up to a maximum of 80 mT/m, at St George's University of London. T1-weighted 3D volume images were acquired using a Turbo Field Echo sequence (TE = 3700ms, TR = 8200ms, flip angle = 8°, providing 160 contiguous sagittal slices with an isotropic voxel dimension of 1mm³ and field-of-view (FOV) of 240x240mm²). Fluid Attenuated Inversion Recovery images (FLAIR) were acquired using an inversion recovery sequence (TE = 125 ms, TR = 11000 ms, TI = 2800 ms with 60 contiguous axial slices of 3 mm slice thickness, FOV = 240 × 240 mm² and voxel dimension 0.96²x3mm³). Diffusion-weighted images (DWI) were acquired using a diffusion sensitised, single-shot spin-echo planar sequence (TE = 75ms, TR = 6450ms, 60 contiguous axial slices, FOV = 224x224mm² in a 112x112 matrix and voxel dimension 2mm³). The first eight DWI volumes were acquired without diffusion sensitisation (b = 0s mm⁻²). The remaining, were obtained with diffusion gradients applied in 32 non-collinear directions (b = 1000s mm⁻²). DWI were simultaneously corrected for the geometric distortions caused by eddy currents and movement artefacts using FSL's 'eddy-correct' (FSL, version 5.0.6, FMRIB, Oxford, <http://fsl.fmrib.ox.ac.uk/fsl/fslwiki/>). Diffusion tensors were computed at every voxel within the DWI using FSL's 'dtifit' [28] and the skull removed using FSL's 'BET' [29]. Fractional Anisotropy (FA) was calculated at every voxel within the diffusion tensor images (DTI), representing the local 'directionality' of diffusion.

Total intracranial volume and white matter hyperintensities. Supratentorial grey matter, white matter and CSF tissues were segmented from the T1-weighted images, and white matter hyperintensities of presumed vascular origin (WMHs) were segmented from the combined tissue intensities from the T1-weighted and FLAIR using a semi-automated procedure adapted from the standard SPM pipeline (SPM version 12, 2014, <https://www.fil.ion.ucl.ac.uk/spm/>). This is described in full in [11,30]. Tissue volumes were quantified by integrating tissue pixel volume contributions within each segmentation, and total intracranial volume was calculated as the sum of grey matter, white matter and CSF volumes. WMH volumes were presented as a percentage of total intracranial volume [11].

Network construction. Brain networks can be regarded as a graph comprising a set of nodes interconnected by a set of edges [31]. In the present study, structural networks were constructed using the workflow shown in Fig 1. Network nodes consisted of 90 anatomical grey matter regions defined using the Automated Anatomical Labelling atlas [32] and network edges consisted of the white matter fibre tracts interconnecting these grey matter regions (traced using deterministic tractography).

Node definition: Native T1-weighted images were co-registered to the b0 in native DTI-space using boundary-based registration using FSL's (FSL version 5.0.6) 'epi-reg' script [33]. The T1-weighted images were normalised to the high resolution T1-weighted Montreal Neurological Institute (MNI) template image [34] provided with MRICro (MRICro, version 6, 2013, www.mricro.com) using a symmetric diffeomorphic non-linear transformation applied via Advanced Normalization Tools [35] (ANTs, version 1.9, <http://stnava.github.io/ANTs/>). These two transformations were combined, inverted and applied to the Automated Anatomical Labelling atlas (excluding the cerebellum) [32] thereby parcellating the native DTI into 90

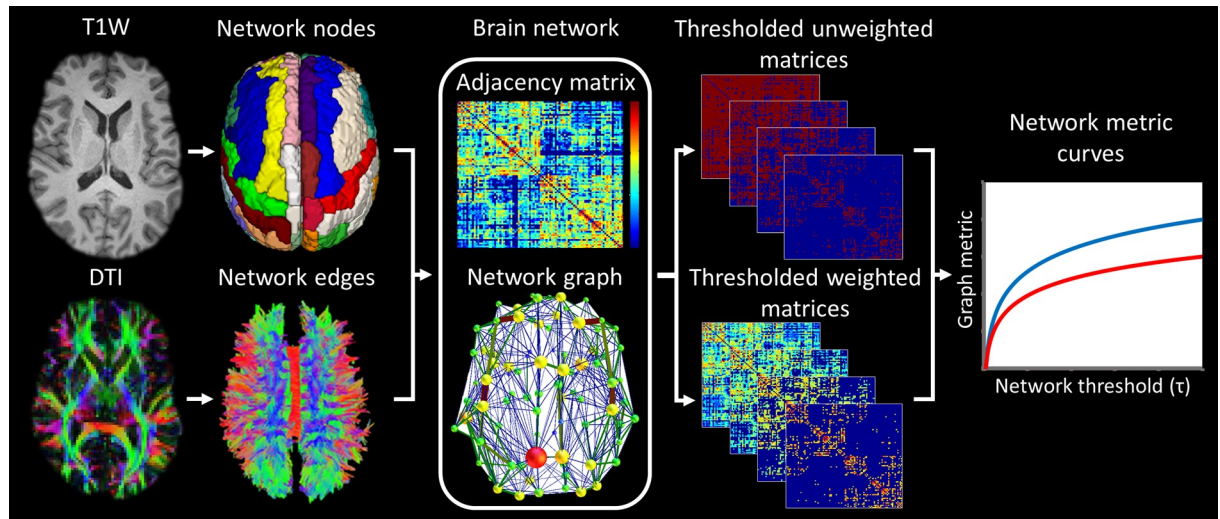


Fig 1. Network construction. The native T1-weighted images were co-registered to the DTI and transformed to Montreal Neurological Institute space. These transforms were combined, inverted and applied to the AAL atlas (excluding cerebellum) parcellating 90 anatomical regions on the DTI (Network nodes). White matter fibre tracts were traced from the DTI (Network edges). Structural networks were defined from the nodes and edges, and the edges weighted by the number of constituent streamlines adjusted for streamline length and end-node volume. Networks were thresholded across 40 edge weighting and edge density thresholds. Weighted and unweighted network metrics were calculated at each threshold and used to construct network metric curves.

<https://doi.org/10.1371/journal.pone.0223297.g001>

supratentorial cortical and subcortical grey matter regions. Each region represented a node of the network.

Edge definition: The trajectory of white matter fibre bundles was reconstructed from the DTI using an in-house deterministic tractography algorithm. The algorithm was seeded across the whole-brain using a super-resolution grid (0.5 mm³) with a step-size of 0.5 mm [36]. Streamlines were terminated if FA dropped below 0.2 or if the angle between principal eigenvectors exceeded 40°. Edges were defined as the presence or absence of a streamline interconnecting node pairs. This resulted in a 90 x 90 adjacency matrix. Weights were ascribed to edges using two weighting strategies with higher weightings given to edges composed of a greater number of tractography streamlines. The two strategies included different corrections for biases inherent to network construction.

Streamline length adjusted weighting strategy: Network weights (w_{ij}^{length}) were defined according to a modified form [21] of Hagmann et al's [37] formula, where l is the length (mm) of the set of N unique streamlines terminating in nodes i and j ,

$$w_{ij}^{length} = \frac{1}{2} \sum_{m=0}^N \frac{1}{l_m}. \tag{1}$$

This method corrects for the distal bias caused by the relationship between length of tractography streamlines and their constituent number (due to longer streamlines containing a greater number of tractography seed points).

Volume-adjusted weighting strategy: Weights (w_{ij}^{vol}) were defined using a modified form of Heuvel and Sporns equation [38], where the number of streamlines terminating in nodes i and j was normalised by the sum of end-node volumes V ,

$$w_{ij}^{vol} = \frac{2N}{(V_i + V_j)}. \tag{2}$$

Larger node volumes contain a greater number of tractography seed points and will therefore have a higher probability of being connected by streamlines. This confound was adjusted for by normalising the number of streamlines by the combined end-node volumes. This method also corrects for localised atrophy of grey matter nodes and for differences in head size.

Summary network metrics. Summary network graph metrics were selected that could be calculated for both weighted and unweighted networks. These described the nodal and global topology of the networks in terms of edge density (unweighted degree), streamline density (weighted degree also known as *strength*), segregation (unweighted and weighted local efficiency), integration (unweighted and weighted nodal efficiency) and nodal influence (unweighted and weighted betweenness centrality). These were computed at each network node using the brain connectivity toolbox (<http://www.brain-connectivity-toolbox.net/>) [39] providing nodal network metrics and averaged across all nodes to provide global network metrics (metric definitions and details can be found in Table 2). Additionally, weighted and unweighted *small-worldness* were quantified—composite measures calculated from the

Table 2. Network metric definitions.

	Unweighted metrics	Weighted metrics
Edge and connection density		
Degree (k)	$k_i = \sum_{j \in N} a_{ij}$, where N is the set of all nodes in the network, (i,j) is an edge connecting nodes i and j , and a_{ij} is the edge connection status between nodes i and j i.e. present = 1, absent = 0.	$k_i^w = \sum_{j \in N} w_{ij}$, where w_{ij} is the normalised edge weight $0 \leq w_{ij} \leq 1$, where normalisation has been performed by dividing weights by the maximum weight in the network.
Segregation		
Local Efficiency (E_{loc})	$E_{loc,i} = \frac{1}{n} \sum_{i \in N} \frac{\sum_{j,h \in N, j \neq i} a_{ij} a_{jh} [d_{jh}(N_i)]^{-1}}{k_i(k_i-1)}$, where $d_{jh}(N_i)$ is the length of the shortest path between j and h , that contains only neighbours of i .	$E_{loc,i}^w = \frac{1}{2} \sum_{i \in N} \frac{\sum_{j,h \in N, j \neq i} (w_{ij} w_{jh} [d_{jh}^w(N_i)]^{-1})^{\frac{1}{3}}}{k_i(k_i-1)}$,
Clustering Coefficient (C)	$C_i = \frac{1}{n} \sum_{i \in N} \frac{2t_i}{k_i(k_i-1)}$, where n is the number of nodes in the network and is the t_i number of triangles around node i , $t_i = \sum_{j,h \in N} a_{ij} a_{jh} a_{jh}$,	$C_i^w = \frac{1}{n} \sum_{i \in N} \frac{2t_i^w}{k_i(k_i-1)}$, where $t_i^w = \sum_{j,h \in N} a_{ij} a_{jh} a_{jh}^w$,
Integration		
Global Efficiency (E)	$E_i = \frac{1}{n} \sum_{i \in N} \frac{\sum_{j \in N, j \neq i} d_{ij}^{-1}}{n-1}$, where d_{ij} is the distance or length of the shortest path between nodes i and j , defined as the number of edges forming the shortest topological route between nodes i and j .	$E_i^w = \frac{1}{n} \sum_{i \in N} \frac{\sum_{j \in N, j \neq i} (d_{ij}^w)^{-1}}{n-1}$, where d_{ij}^w is the distance or length of the shortest path between nodes i and j , defined as the sum of the inverse of weights forming the shortest topological route between nodes i and j .
Characteristic Path Length (L)	$L_i = \frac{1}{n} \sum_{i \in N} \frac{\sum_{j \in N, j \neq i} d_{ij}}{n-1}$,	$L_i^w = \frac{1}{n} \sum_{i \in N} \frac{\sum_{j \in N, j \neq i} d_{ij}^w}{n-1}$,
Nodal influence		
Betweenness Centrality (b)	$b_i = \frac{1}{(n-1)(n-1)} \sum_{h,j \in N} \frac{\rho_{hi}^{(i)} \rho_{hj}^{(i)}}{\rho_{hj}}$, $h \neq j, h \neq i, j$ where ρ_{hj} is the number of shortest paths between nodes h and j , and $\rho_{hi}^{(i)}$ is the number of shortest paths that pass through node i .	$b_{ij}^w = \frac{1}{(n-1)(n-1)} \sum_{h,j \in N} \frac{\rho_{hi}^{(i)} \rho_{hj}^{(i)}}{\rho_{hj}}$, $h \neq j, h \neq i, j$
Small-world structure		
Small-worldness (S)	$S = \frac{C_{rand} / C_{rand}}{L_{rand} / L_{rand}}$, where C_{rand} and L_{rand} are the average unweighted clustering coefficient and average unweighted characteristic path length computed on 100 randomly re-wired networks.	$S^w = \frac{C_{rand}^w / C_{rand}^w}{L_{rand}^w / L_{rand}^w}$, where C_{rand}^w and L_{rand}^w are the average weighted clustering coefficient and average weighted characteristic path length computed on 100 randomly re-wired networks.

<https://doi.org/10.1371/journal.pone.0223297.t002>

characteristic path length and clustering coefficient normalised by the equivalent metrics computed over 100 randomly re-wired networks [40]. Networks were considered to have ‘small-world’ topological properties when unweighted or weighted *small-worldness* $\gg 1$.

Adapted from [39].

Network thresholding. The networks were thresholded so that low weight network edges that are likely to have been generated by noise within the DTI data, were removed. The choice of threshold is largely arbitrary [41]. Additionally, the topological properties of a network are highly dependent on the number of edges in the network, therefore, it is necessary to control for edge density when evaluating network topology [42]. Consequently, all network metrics were assessed at 40 evenly-spaced fixed levels of edge density except for unweighted degree, itself an indicator of edge density, which was assessed across 40 fixed levels of edge weighting. The upper edge density threshold was determined by the maximum value at which all subjects’ networks could be successfully density-matched. Edge weighting thresholds were set as the average edge weight for the average subject at each density threshold.

Network metric curves were constructed by plotting the network metric value at each network threshold. At high edge weighting thresholds and low edge density thresholds, low weight edges will have been removed, meaning that hub nodes will have a greater influence over the network metrics at these thresholds.

Statistical analysis

Between-group differences in WMHs and total intracranial volume were tested using ANCOVAs. WMHs were \log_{10} -transformed to correct for non-Gaussianity prior to analysis. Between-group differences in nodal and global network graph metrics were tested for the total area under each metric curve (AUC_{total}) and at every point along the metric curve (*point-by-point*). This latter method was used to verify the AUC_{total} results and to determine which network thresholds were primarily contributing to significant effects. For the AUC_{total} method, between-group comparisons were performed using parametric (Gaussian data and data that could be \log_{10} -transformed to Gaussian) and non-parametric permutation ANCOVAs with 10000 permutations (non-Gaussian data), performed using SPSS version 24 (IBM Corp, 2015) and FSL’s randomise (FSL version 5.0.6) (Winkler *et al.*, 2014), respectively. Residuals were checked for gaussianity using histograms and quantile-quantile plots. Results were Bonferroni corrected for multiple comparisons. Statistical testing for the *point-by-point* analyses was performed using permutation ANCOVAs and corrected for multiplicity across the network thresholds using the multi-threshold permutation correction (MTPC) method [43,44] performed using in-house software. For results to be considered significant they were required to exceed the familywise error (FWE) adjusted critical threshold and the area under the curve (AUC_{MTPC}) of supra-critical clusters of results had to exceed the average AUC_{MTPC} of supra-critical clusters for the null distribution. Clusters were required to be formed by a minimum of three consecutive network thresholds. Within-group correlations with cognitive (executive function, episodic memory, processing speed, working memory, MMSE) and disease severity indices (FSRP, pack years smoked, exacerbation frequency, FEV₁% pred., FVC % pred., PO₂, PCO₂ and SGRQ) were tested for the AUC_{total} analyses using partial Spearman’s Rho correlations in SPSS version 24 (IBM Corp, 2015). Correlation results were Bonferroni corrected for the number of statistical comparisons made per cognitive function or disease severity measure.

Age and sex were included as covariates of no interest in all statistical models, hereafter referred to as *confounders*. Additionally, estimated pre-morbid IQ was included in any within-group correlative model testing relationships with cognition, and total intracranial volume in all analyses using the streamline length-adjusted weighting strategy as this method did not

already include a correction for head size. Pack years smoking history and anxiety and depression (HADS—total) were strongly related to group membership, therefore, it was not possible to control for these *confounders* in the statistical models. Subjects with missing cognitive or disease severity data, were excluded ‘pairwise’ from correlation analyses.

Results

Macrostructural brain measures

COPD patients had significantly greater normalised WMH volumes, Median (IQR) = 0.85 (1.41)% than controls = 0.40 (0.43)%, ($F(1,49) = 5.34, p = 0.025$). There were no group differences in total intracranial volume (COPD patients, average \pm SD = 1440 \pm 99, controls = 1427 \pm 81, $F(1,24) = 2.619, p = 0.112$). These results have been reported elsewhere [11].

Global network analysis

The structural brain networks of all 30 patients with COPD and 23 control subjects showed ‘small-world’ topological properties (unweighted and weighted *small-worldness* $\gg 1$) across all network thresholds for both the streamline length-adjusted weighting strategy and the volume-adjusted weighting strategy (see S1 and S2 Figs). A ‘small-world’ network configuration is characterised by high clustering of local connections with a few long-range connections mediating a short path length and is thought to provide the optimal balance between modular specialisation and distributed information processing [20,31,45].

Between-group comparisons of global unweighted and weighted network metrics for the streamline length-adjusted weighting strategy made using the total AUC_{total} method are shown in Table 3. Table 4 shows the equivalent results for the comparisons made *point-by-point* along each metric curve.

Table 3. Group comparison of global network metrics—total area under the metric curve (AUC_{total}).

Unweighted Network Metrics	Controls	COPD	$F(df_1, df_2)$	p
Degree	154.89 (33.43)	122.76 (57.07)	8.953 ² (1,48)	0.044 ^{2b*}
Global Efficiency ($\times 10^{-2}$)	5.88 \pm 0.08	5.91 \pm 0.11	1.164 ¹ (1,48)	1.000 ^{1b}
Local Efficiency ($\times 10^{-2}$)	8.30 \pm 0.31	8.15 \pm 0.36	1.526 ¹ (1,48)	1.000 ^{1b}
Betweenness Centrality	23.00 \pm 1.59	22.93 \pm 5.16	0.020 ¹ (1,48)	1.000 ^{1b}
Small-worldness ($\times 10^{-1}$)	5.53 (1.10)	5.69 (1.36)	0.017 ³ (1,48)	0.896 ^{3b}
Weighted Network Metrics				
Degree	36.31 \pm 4.74	30.78 \pm 5.89	9.584 ¹ (1,48)	0.033 ^{1b*}
Global Efficiency ($\times 10^{-3}$)	6.33 \pm 1.27	6.48 \pm 1.44	1.177 ¹ (1,48)	1.000 ^{1b}
Local Efficiency ($\times 10^{-3}$)	7.99 \pm 1.61	7.91 \pm 1.81	0.431 ¹ (1,48)	1.000 ^{1b}
Betweenness Centrality	45.06 (7.63)	45.53 (7.54)	0.479 ² (1,48)	1.000 ^{2b}
Small-worldness ($\times 10^{-1}$)	6.03 (1.29)	6.34 (1.60)	0.224 ³ (1,48)	0.474 ^{3b}

Group comparison of global network measures using the total area under the metric curves. Age, sex and total intracranial volume were included as confounders in all analyses. Group means \pm standard deviations are presented for Gaussian data, and medians (interquartile ranges) for non-Gaussian data.

¹Gaussian and

² \log_{10} -transformed to Gaussian data were assessed using parametric ANCOVAs and non-Gaussian data by

³non-parametric permutation ANCOVAs (10000 permutations). F -statistics (F), degrees of freedom (df) and p -values (p) are displayed.

^bBonferroni corrected p -values.

*significant at $p < 0.05$.

<https://doi.org/10.1371/journal.pone.0223297.t003>

Table 4. Group comparison of global network metrics—‘point-by-point’ along the metric curve.

Unweighted Network Metrics	Peak statistics			Cluster		
	t_{max} (df)	p_{FWE}	τ	AUC _{MTPC}	AUC _{crit}	MTPC _{sig}
Degree	3.706 (48)	0.004	17.427	15.408	5.384	Y
Global Efficiency	-2.272 (48)	0.348	0.110	-	0.002	N
Local Efficiency	2.203 (48)	0.369	0.059	-	0.003	N
Betweenness Centrality	-1.787 (48)	0.648	0.017	-	0.003	N
Small-worldness	-1.817 (48)	0.660	0.021	-	0.003	N
Weighted Network Metrics						
Degree	3.216 (48)	0.006	0.169	0.128	0.040	Y
Global Efficiency	-2.335 (48)	0.098	0.017	-	0.014	N
Local Efficiency	-1.779 (48)	0.420	0.021	-	0.009	N
Betweenness Centrality	-1.775 (48)	0.581	0.017	-	0.004	N
Small-worldness	-1.970 (48)	0.526	0.165	-	0.004	N

Point-by-point group comparison of global network measures. Age, sex and total intracranial volume were included as confounders in all analyses. For the maximum statistical difference (Peak), the t -statistic (t_{max}), degrees of freedom (df), permutation-based family-wise error corrected p -value (p_{FWE}) and the network threshold at which this difference occurs (τ) are reported under the heading ‘Peak statistics’. Additionally, the size of supra-critical clusters (AUC_{MTPC}), the critical threshold for these clusters (AUC_{crit}) and the significance (MTPC_{sig}), Y = yes, N = no are reported under the heading ‘Cluster’.

<https://doi.org/10.1371/journal.pone.0223297.t004>

Results for the streamline length-adjusted weighting strategy were broadly analogous between the AUC_{total} and *point-by-point* analysis approaches, with both showing that COPD patients had significantly reduced average weighted and unweighted degree compared to controls (see Tables 3 and 4). This indicates that COPD patients’ brain networks contained fewer edges and that edges were generally *weaker* i.e. composed of fewer streamlines. However, the *point-by-point* approach also showed that, whilst patients with COPD had significantly reduced average weighted degree across all network thresholds, differences in average unweighted degree were confined to low edge weighting thresholds. These findings suggest that the brain networks of COPD patients contain fewer *weak* network edges but a similar number of *strong* edges to those present in controls (Fig 2 and Table 4). Use of the volume-adjusted weighting strategy removed the significance of the group differences in the AUC_{total} of average weighted and unweighted degree, although a trend remained, $F(1,49) = 7.722, p = 0.080$ and $F(1,49) = 8.016, p = 0.067$, respectively (see S1 Table), however, both remained significant using the *point-by-point* approach ($t_{max}(49) = 3.653, p = 0.005$ and $t_{max}(49) = 2.822, p = 0.018$, respectively, see S2 Table).

There were no other significant group differences for the remaining weighted or unweighted global network metrics, including: global efficiency, local efficiency, betweenness centrality or *small-worldness*, regardless of the edge weighting strategy used (Tables 3 and 4 and S1 and S2 and S1 and S2 Figs).

Nodal network analysis

The spatial pattern of trends in the weighted nodal metrics for the streamline length-adjusted weighting strategy using the AUC_{total} method can be viewed in Fig 3. An equivalent figure for the unweighted metric results and for the volume-adjusted weighting strategy can be found in the S3 and S4 Figs. There was a general trend for patients with COPD to have numerically lower weighted and unweighted nodal degree (71/90 and 70/90 of nodes, respectively), and numerically higher weighted nodal efficiency (72/90 nodes). However, the only significant difference occurred for the nodal unweighted degree in the right hemispheric superior temporal

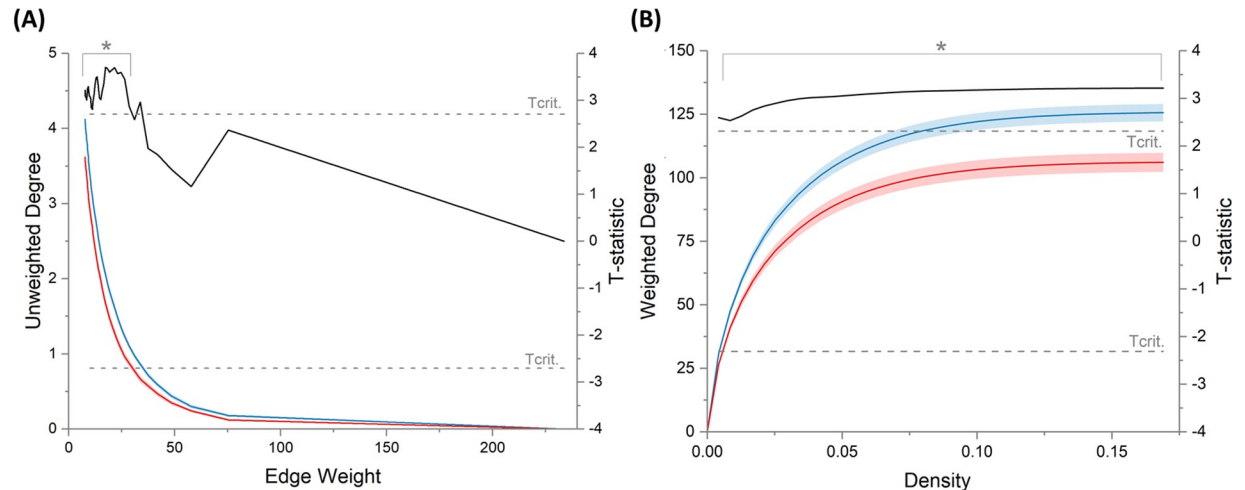


Fig 2. Group comparison of unweighted degree (A) and weighted degree (B) made point-by-point along the metric curve. Group average metric curves are plotted on the left axes. Red = COPD, Blue = Controls. Shaded error bars represent the standard error of the mean. T-statistics (black) are plotted on the right axis. Two-tailed critical thresholds (T_{crit}) are indicated by dashed grey lines. *significant at $P_{FWE} < 0.05$ after MTPC correction for multiplicity.

<https://doi.org/10.1371/journal.pone.0223297.g002>

gyrus, with COPD patients having lower unweighted degree than controls ($t(48) = -3.961$, $p = 0.016$). This result did not survive correction for end-node volume. No nodal group differences were found using the MTPC method.

Correlations with cognitive function and disease severity

There were no significant partial spearman's rho correlations for weighted or unweighted global network measures and disease severity or cognitive function for either subject group, regardless of the edge weighting strategy used (Tables 5 and S4–S6).

Discussion

This study used deterministic tractography and structural network analysis to investigate cross-sectionally whether there are any differences in the pattern of white matter connectivity between people with COPD and control subjects. Both subject groups' networks had the expected 'small-world' topology, with high clustering of local connections and short path length. Globally, COPD patients' networks were found to have reduced white matter connectivity both in terms of the number of network edges and the *strength* of these edges (the adjusted number of constituent tractography streamlines). Analysis on a *point-by-point* basis indicated that the strength of network edges was reduced across all levels of network density, whereas the difference in the number of edges only occurred at low edge weighting thresholds. This suggests that whilst both *strong* and *weak* network edges were impaired, only *weak* edges were disconnected entirely. In contrast, there were no significant group differences in the topological organisation of the networks (i.e. no difference in network integration, segregation, nodal influence or *small-worldness*), this suggests that there is sufficient redundancy to accommodate a reduction in connectivity without compromising the organisational efficiency of the overall network structure. These results appear to have been driven by subtle (and largely sub-significant) group differences across the majority of network nodes. Adjusting for differences in end-node volume (volume-adjusted weighting strategy) removed the significance of group differences in average unweighted and weighted degree when measured as the total area under

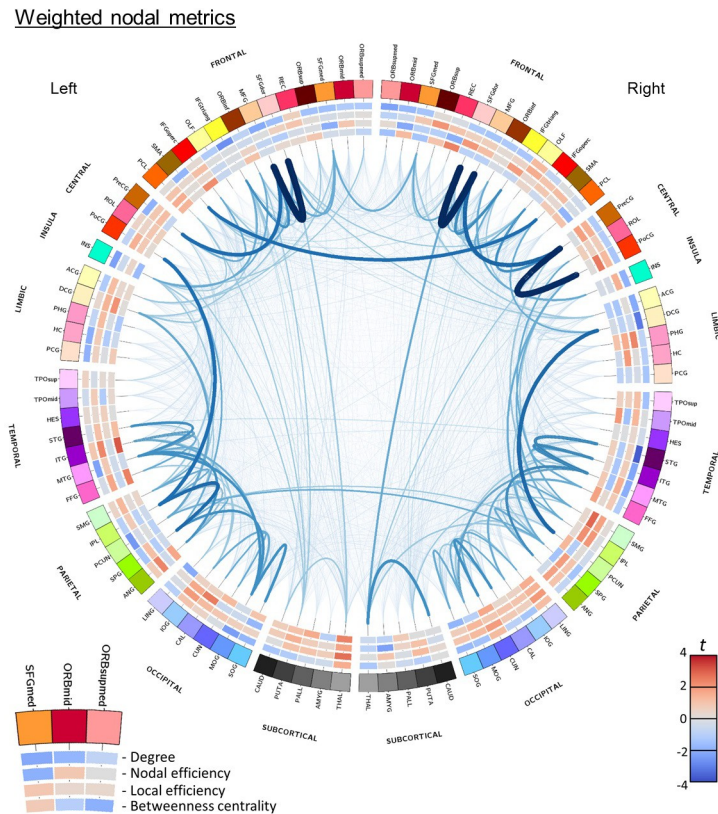


Fig 3. Circular representation of network connections in all subjects and between-group differences in weighted nodal network metrics. Network nodes are arranged around the outermost circle and assigned a unique colour. Nodes are split by hemisphere (right hemisphere on the right) and grouped within the macroscopic subdivisions defined in [32] (Frontal, Central, Insula, Limbic, Temporal, Parietal, Occipital, Subcortical). Within these subdivisions nodes are arranged by structural laterality. S3 Table summarises the node name abbreviations. The inner four circles show red-blue t -statistic heatmaps for the sub-significant between-group AUC_{total} trends in nodal weighted metrics for the contrast COPD > Controls. Connections represent the edges present in any subject. The thickness and darkness of connections indicates the average edge weight for the streamline length-adjusted weighting strategy.

<https://doi.org/10.1371/journal.pone.0223297.g003>

the metric curves, however, they remained significant when using the *point-by-point* approach. This suggests that even if local cerebral atrophy contributed to these group differences it is unlikely to be fully responsible for them. There were no other notable differences between the results from the two weighting strategies. No significant relationships were found between global network metrics and measures of cognitive function or disease severity, so it cannot be determined whether or not loss of connectivity was responsible for cognitive dysfunction in this cohort.

To our knowledge this is the first study to use structural network analysis to examine white matter connectivity in people with COPD. However, the finding of reductions in white matter connectivity in COPD compared to controls are consistent with reports of widespread tract-based increases in diffusivity and decreases in anisotropy, found both in this and other COPD cohorts [10,12,13], suggestive of a deterioration in the white matter in COPD. Such diffusion abnormalities are consistent with those found in other chronic diseases with a high prevalence of mild cognitive impairment, including diabetes, hypertension and chronic kidney disease e.g. [16,46–50]. A previous study of the present cohort found increases in functional connectivity, encompassing all resting-state networks except the visual network [10]. It is plausible

Table 5. Within-group correlations between global weighted network metrics and cognitive and disease severity measures.

	Weighted Global Network Metrics									
	Degree		Global Efficiency		Local Efficiency		Betweenness Centrality		Small-worldness	
	<i>rho</i> (df)	<i>p</i>	<i>rho</i> (df)	<i>p</i>	<i>rho</i> (df)	<i>p</i>	<i>rho</i> (df)	<i>p</i>	<i>rho</i> (df)	<i>p</i>
Controls (N = 23)										
Executive Function	0.561 (18)	0.100 ^b	-0.007 (18)	1.000 ^b	-0.078 (18)	1.000 ^b	0.265 (18)	1.000 ^b	0.176 (18)	1.000 ^b
Episodic Memory	0.003 (18)	1.000 ^b	-0.085 (18)	1.000 ^b	0.079 (18)	1.000 ^b	-0.367 (18)	1.000 ^b	0.510 (18)	0.220 ^b
Processing Speed	0.337 (18)	1.000 ^b	-0.049 (18)	1.000 ^b	-0.080 (18)	1.000 ^b	-0.133 (18)	1.000 ^b	0.410 (18)	0.720 ^b
Working Memory	0.452 (18)	0.460 ^b	-0.071 (18)	1.000 ^b	-0.108 (18)	1.000 ^b	0.019 (18)	1.000 ^b	0.156 (18)	1.000 ^b
MMSE	0.054 (18)	1.000 ^b	-0.283 (18)	1.000 ^b	-0.078 (18)	1.000 ^b	-0.012 (18)	1.000 ^b	0.194 (18)	1.000 ^b
COPD (N = 30)										
Executive Function	-0.238 (25)	1.000 ^b	0.225 (25)	1.000 ^b	0.105 (25)	1.000 ^b	-0.170 (25)	1.000 ^b	-0.245 (25)	1.000 ^b
Episodic Memory	-0.006 (25)	1.000 ^b	-0.330 (25)	0.930 ^b	-0.390 (25)	0.440 ^b	-0.366 (25)	0.600 ^b	-0.110 (25)	1.000 ^b
Processing Speed	-0.138 (25)	1.000 ^b	-0.101 (25)	1.000 ^b	-0.112 (25)	1.000 ^b	-0.149 (25)	1.000 ^b	-0.107 (25)	1.000 ^b
Working Memory	0.025 (25)	1.000 ^b	0.065 (25)	1.000 ^b	0.005 (25)	1.000 ^b	-0.237 (25)	1.000 ^b	-0.237 (25)	1.000 ^b
MMSE	0.049 (25)	1.000 ^b	0.108 (25)	1.000 ^b	0.233 (25)	1.000 ^b	0.015 (25)	1.000 ^b	0.291 (25)	1.000 ^b
FSRP	-0.081 (26)	1.000 ^b	-0.018 (26)	1.000 ^b	-0.043 (26)	1.000 ^b	0.157 (26)	1.000 ^b	0.098 (26)	1.000 ^b
Pack Years	-0.067 (26)	1.000 ^b	0.098 (26)	1.000 ^b	0.186 (26)	1.000 ^b	-0.047 (26)	1.000 ^b	-0.095 (26)	1.000 ^b
Exacerbation Frequency	0.033 (26)	1.000 ^b	-0.278 (26)	1.000 ^b	-0.224 (26)	1.000 ^b	-0.110 (26)	1.000 ^b	0.318 (26)	1.000 ^b
FEV ₁ (% pred.)	0.139 (26)	1.000 ^b	-0.446 (26)	0.200 ^b	-0.403 (26)	0.370 ^b	-0.045 (26)	1.000 ^b	0.093 (26)	1.000 ^b
FVC (% pred.)	0.144 (26)	1.000 ^b	-0.311 (26)	1.000 ^b	-0.199 (26)	1.000 ^b	-0.275 (26)	1.000 ^b	0.368 (26)	0.590 ^b
PO ₂	-0.135 (26)	1.000 ^b	-0.074 (26)	1.000 ^b	-0.045 (26)	1.000 ^b	-0.075 (26)	1.000 ^b	-0.012 (26)	1.000 ^b
PCO ₂	0.092 (26)	1.000 ^b	0.353 (26)	0.650 ^b	0.250 (26)	1.000 ^b	0.146 (26)	1.000 ^b	-0.032 (26)	1.000 ^b
SGRQ	0.068 (26)	1.000 ^b	0.223 (26)	1.000 ^b	0.239 (26)	1.000 ^b	0.082 (26)	1.000 ^b	-0.010 (26)	1.000 ^b

Age, sex and total intracranial volume were entered as confounders in all analyses. Additionally, estimated pre-morbid IQ was included in correlations involving cognitive function. Spearman's correlation coefficients (*rho*), and *p*-values (*p*) are displayed.

^bBonferroni corrected *p*-values.

<https://doi.org/10.1371/journal.pone.0223297.t005>

that this increase in functional connectivity reflects an over-recruitment of the surviving network structure in order to compensate for the loss of white matter connectivity.

Since no relationships were found with clinical disease severity measures in this study, it is difficult to draw any mechanistic conclusions about the pathophysiological causes of this network disruption. However, a number of conventional anatomical MR imaging markers of cerebral SVD, including small subcortical infarcts, WMHs, cerebral microbleeds and brain atrophy (including generalised atrophy, ventriculomegaly, hippocampal atrophy and focal atrophy) [51] have been identified in COPD [8–10,13,52–54] or found to be associated with reduced lung function [55–58]. Furthermore, cardiovascular risk factors which are thought to predispose development of arteriosclerosis (otherwise known as age-related cardiovascular risk-factor-related SVD) are also commonly found in COPD—most notably elderly age, diabetes, hypertension and smoking [51,59,60]. Additionally, COPD itself is an independent risk factor for cardiovascular disease [61]. Consequently, it has been hypothesised that SVD is responsible for the neuropathology and cognitive impairment found in COPD [8,9,11,62].

Previous network studies of SVD have reported reductions in the density and *strength* of network edges [21,63] consistent with those found in the present study. However, they also report more profound alterations to network topology not present in this study, such as reductions in network integration and segregation [21,62,63]. These topological changes have been found to mediate the relationship between DTI measures of white matter deterioration and cognitive impairment (executive function and processing speed) [21]. Therefore, the lack of substantial disruption in network topology in the present cohort may account for the mildness

of their cognitive impairment (only one patient met the MMSE criteria for severe cognitive impairment) as their brain networks are able to accommodate a loss of connections without compromising the overall efficiency of the network. Nevertheless this loss of connections is likely to increase the vulnerability of the networks to future damage and increase the risk of further cognitive decline. The potential utility of brain MR features as early prognostic markers of cognitive decline and dementia onset have been demonstrated in other diseases [64–67]. For instance, a prospective study showed that longitudinal change in MR measures, including increase in WMHs and worsening of white matter tissue microstructure (measured using DTI) were predictive of conversion to dementia in SVD, despite there being no detectable change on neuropsychological testing [66]. Furthermore, longitudinal decline in white matter connectivity was found to mediate many of the relationships between progression of conventional brain MR and DTI markers of SVD and conversion to dementia [67]. Future investigation of longitudinal change in white matter connectivity in COPD may help predict which patients are at greater risk of developing cognitive impairment and dementia, enabling personalised treatment and support.

The lack of direct relationships between cognitive and network measures in the present study is perhaps surprising, given that a number of other studies have reported relationships between disruption of large-scale structural brain networks and reduced cognitive function e.g. [21,63, 68,69]. This may reflect the relatively small cohort size in this study and/or the mild severity of the COPD (moderate-severe airflow obstruction without significant hypoxaemia or hypercapnia) in this study. Brain reserve capacity [70] and cognitive reserve [71] have been proposed to explain similar disparities in brain pathology and functional outcome [71,72]. These related concepts suggest that an individual's trajectory of cognitive decline is moderated by factors, such as the amount of physical substrate available (e.g. brain size, number of neurons) and how effectively they can utilise their brain networks (e.g. cognitive efficiency and flexibility) [72]; this may affect their resilience to accumulating pathology. In this study estimated pre-morbid IQ and total intracranial volume were included as covariates in statistical analyses as surrogates for cognitive reserve [73] and brain reserve e.g. [74]. However, it is possible that residual effects remained. A number of disease-related factors and co-morbidities including anxiety and depression [75,76], disturbed sleep [76,77] and reduced physical activity [78,79] may also be contributing to functional impairment without commensurate effects on white matter structure. Further research is required to elucidate the relationship between disease-related factors, changes in white matter connectivity and cognitive impairment in COPD.

Limitations

The main limitation of this study was that it was not possible to adequately control for smoking history, hypertension or anxiety and depression in the between-group analysis due to the strong dependence of number of pack years smoked and total HADS score on group-membership, and the lack of available blood pressure data. Consequently, it was not possible to exclude these disease factors as being responsible for the network disruption. This is particularly significant as previous studies have reported DTI and/or structural and functional network abnormalities to occur with these conditions e.g. [16,80–82]. No formal power calculation was performed prior to data acquisition. The sample size is relatively small, although comparable in size to other studies that have reported group differences in MR imaging measures in COPD [10,13,53,83], limiting the generalisability of these findings to other COPD cohorts. This study used composite measures of cognition to test for correlations with network measures. This is a common approach used e.g. [21,63,84], however, it is possible that individual neuropsychological sub-tests would have been more sensitive to network disruption.

Diffusion MR remains the only non-invasive in vivo method for investigating white matter connectivity. With deterministic tractography the uncertainty of the principal direction of diffusion in areas of low FA (e.g. in WMHs) or complex fibre anatomy (e.g. the crossing, bending, and kissing fibres prevalent in the optic radiation, callosal fibres, pyramidal tracts [85]) lead to errors which accumulate along the length of the tractography streamline. The present study aimed to reduce these effects by only seeding the deterministic tractography algorithm within areas with a well-defined principal diffusion direction ($FA \geq 0.2$) [21] and by using super-resolution seeding to reduce partial-volume effects [36]. Application of probabilistic tractography (e.g. [86]) and/or a correction for cerebrospinal fluid contamination may improve tracking through areas of low FA [87,88] such as the WMHs present in this cohort and areas of partial-voluming with cerebrospinal fluid. However, probabilistic tractography is more computationally demanding and has an elevated risk of producing false-positive connections [89]. Constrained spherical deconvolution [90,91] based tractography could also be used to overcome some of these effects, but has limited applicability to the present data which used relatively few diffusion directions at $b = 1000 \text{ s mm}^{-2}$ [92].

Conclusions

This study has provided a cross-sectional analysis of differences in white matter connectivity between COPD patients with mild-moderate airflow obstruction and age and sex-matched controls. Compared to controls, COPD patients had under-connected structural networks comprising fewer and *weaker* network connections, but with their topological organisation conserved. It was not possible to remove the confounding effects of smoking history and hypertension, so it could not be determined whether this was COPD-related effect *per se*, or whether it was the result of COPD patients having greater cardiovascular risk.

Supporting information

S1 Table. Group comparison of global network metrics for the volume-adjusted weighting strategy—total area under the metric curve. Group comparison of global network measures using the total area under the metric curves. Age and sex were included as confounders in all analyses. Group means \pm standard deviations are presented for Gaussian data, and medians (interquartile ranges) for non-Gaussian data. ¹Gaussian and ² \log_{10} -transformed to Gaussian data were assessed using parametric ANCOVAs and non-Gaussian data by ³non-parametric permutation ANCOVAs (10000 permutations). *F*-statistics, degrees of freedom (df_1 , df_2) and *p*-values are displayed.

(DOCX)

S2 Table. Group comparison of global network metrics for the volume-adjusted weighting strategy—‘point-by-point’ along the metric curve. Point-by-point group comparison of global network measures. Age and sex were included as confounders in all analyses. For the maximum statistical difference (Peak), the *t*-statistic (t_{max}), degrees of freedom (*df*), permutation-based family-wise error corrected *p*-value (p_{FWE}) and the network threshold at which this difference occurs (τ) are reported under the heading ‘Peak statistics’. Additionally, the size of supra-critical clusters (AUC_{MTPC}), the critical threshold for these clusters (AUC_{crit}) and their significance ($MTPC_{sig}$), Y = yes, N = no are reported under the heading ‘Cluster’.

(DOCX)

S3 Table. List of network nodes and abbreviations for the circular network diagrams.

(DOCX)

S4 Table. Within-group correlations between global unweighted network metrics and cognitive and disease severity measures for the streamline length-adjusted weighting strategy.

Age, sex and total intracranial volume were entered as confounder in all analyses. Additionally, estimated pre-morbid IQ was included in correlations involving cognitive function. Spearman's correlation coefficients (ρ), degrees of freedom (df) and p -values (p) are displayed.

^bBonferroni corrected p -values. =

(DOCX)

S5 Table. Within-group correlations between global weighted network metrics and cognitive and disease severity measures for the volume-adjusted weighting strategy.

Age and sex were entered as confounders in all analyses. Additionally, estimated pre-morbid IQ was included in correlations involving cognitive function. Spearman's correlation coefficients (ρ), degrees of freedom (df) and p -values (p) are displayed. ^bBonferroni corrected p -values.

(DOCX)

S6 Table. Within-group correlations between global unweighted network metrics and cognitive and disease severity measures for the volume-adjusted weighting strategy.

Age and sex were entered as confounders in all analyses. Additionally, estimated pre-morbid IQ was included in correlations involving cognitive function. Spearman's correlation coefficients (ρ), degrees of freedom (df) and p -values (p) are displayed. ^bBonferroni corrected p -values.

(DOCX)

S1 Fig. Group comparison of unweighted (left column) and weighted (right column) global network metrics made point-by-point along the metric curve for the streamline length-adjusted weighting strategy.

Group average metric curves for unweighted and weighted global network metrics are plotted on the left axes. Red = COPD patients, Blue = Controls. Shaded error bars represent the standard error of the mean. T -statistics (black) are plotted on the right axis. Two-tailed critical thresholds (T_{crit}) are indicated by dashed grey lines.

(PDF)

S2 Fig. Group comparison of unweighted (left column) and weighted (right column) global network metrics made point-by-point along the metric curve for the volume-adjusted weighting strategy.

Group average metric curves for unweighted and weighted global network metrics are plotted on the left axes. Red = COPD patients, Blue = Controls. Shaded error bars represent the standard error of the mean. T -statistics (black) are plotted on the right axis.

Two-tailed critical thresholds (T_{crit}) are indicated by dashed grey lines. *significant at

$P_{FWE} < 0.05$ after MTPC correction for multiplicity.

(PDF)

S3 Fig. Circular representation of network connections in all subjects and between-group differences in unweighted nodal network metrics for the streamline length-adjusted weighting strategy.

Network nodes are arranged around the outermost circle and assigned a unique colour. Nodes are split by hemisphere (right hemisphere on the right) and grouped within the macroscopic subdivisions defined in [32] (Frontal, Central, Insula, Limbic, Temporal, Parietal, Occipital, Subcortical). Within these subdivisions nodes are arranged by structural laterality. S3 Table summarises the node name abbreviations. The inner four circles show red-blue t -statistic heatmaps for between-group AUC_{total} differences in nodal unweighted metrics for the contrast COPD patients > controls. Connections represent the edges present in any subject. The thickness and darkness of connections indicates the average edge weight for the streamline length-adjusted weighting strategy. Significant results are outlined in black.

(TIF)

S4 Fig. Circular representation of network connections in all subjects and between-group differences in nodal network metrics for the volume-adjusted weighting strategy. Network nodes are arranged around the outermost circle and assigned a unique colour. Nodes are split by hemisphere (right hemisphere on the right) and grouped within the macroscopic subdivisions defined in [32] (Frontal, Central, Insula, Limbic, Temporal, Parietal, Occipital, Subcortical). Within these subdivisions nodes are arranged by structural laterality. S3 Table summarises the node name abbreviations. The inner four circles show red-blue t-statistic heatmaps for the sub-significant between-group AUC_{total} trends in nodal unweighted metrics for the contrast COPD patients > controls. Connections represent the edges present in any subject. The thickness and darkness of connections indicates the average edge weight for the volume-adjusted weighting strategy.

(TIF)

S1 File. Study data.

(XLSX)

Author Contributions

Conceptualization: Paul W. Jones, James W. Dodd, Thomas R. Barrick.

Data curation: Catherine A. Spilling.

Formal analysis: Catherine A. Spilling.

Funding acquisition: Paul W. Jones.

Investigation: Catherine A. Spilling, James W. Dodd.

Methodology: Catherine A. Spilling, Thomas R. Barrick.

Supervision: Paul W. Jones, James W. Dodd, Thomas R. Barrick.

Visualization: Catherine A. Spilling.

Writing – original draft: Catherine A. Spilling.

Writing – review & editing: Catherine A. Spilling, Paul W. Jones, James W. Dodd, Thomas R. Barrick.

References

1. Kodl CT, Seaquist ER. Cognitive Dysfunction and Diabetes Mellitus. *Endocr Rev.* 2008; 29: 494–511. <https://doi.org/10.1210/er.2007-0034> PMID: 18436709
2. Berger I, Wu S, Masson P, Kelly PJ, Duthie FA, Whiteley W, et al. Cognition in chronic kidney disease: a systematic review and meta-analysis. *BMC Med.* 2016; 14. <https://doi.org/10.1186/s12916-016-0745-9> PMID: 27964726
3. Meade T, Manolios N, Cumming SR, Conaghan PG, Katz P. Cognitive Impairment in Rheumatoid Arthritis: A Systematic Review. *Arthritis Care Res.* 2018; 70: 39–52. <https://doi.org/10.1002/acr.23243> PMID: 28371512
4. Agusti A, Calverley PM, Celli B, Coxson HO, Edwards LD, Lomas DA, et al. Characterisation of COPD heterogeneity in the ECLIPSE cohort. *Respir Res.* 2010; 11: 122. <https://doi.org/10.1186/1465-9921-11-122> PMID: 20831787
5. Dodd JW. Lung disease as a determinant of cognitive decline and dementia. *Alzheimers Res Ther.* 2015; 7: 32. <https://doi.org/10.1186/s13195-015-0116-3> PMID: 25798202
6. Chang SS, Chen S, McAvay GJ, Tinetti ME. Effect of Coexisting Chronic Obstructive Pulmonary Disease and Cognitive Impairment on Health Outcomes in Older Adults. *J Am Geriatr Soc.* 2012; 60: 1839–1846. <https://doi.org/10.1111/j.1532-5415.2012.04171.x> PMID: 23035917

7. Antonelli Incalzi R. Verbal memory impairment in COPD: its mechanisms and clinical relevance. *CHEST J.* 1997; 112: 1506. <https://doi.org/10.1378/chest.112.6.1506> PMID: 9404746
8. van Dijk EJ. Arterial oxygen saturation, COPD, and cerebral small vessel disease. *J Neurol Neurosurg Psychiatry.* 2004; 75: 733–736. <https://doi.org/10.1136/jnnp.2003.022012> PMID: 15090569
9. Lahousse L, Vernooij MW, Darweesh SKL, Akoudad S, Loth DW, Joos GF, et al. Chronic obstructive pulmonary disease and cerebral microbleeds. The Rotterdam study. *Am J Respir Crit Care Med.* 2013; 188: 783–788. <https://doi.org/10.1164/rccm.201303-0455OC> PMID: 23885754
10. Dodd JW, Chung AW, van den Broek MD, Barrick TR, Charlton RA, Jones PW. Brain Structure and Function in Chronic Obstructive Pulmonary Disease: A Multimodal Cranial Magnetic Resonance Imaging Study. *Am J Respir Crit Care Med.* 2012; 186: 240–245. <https://doi.org/10.1164/rccm.201202-0355OC> PMID: 22652026
11. Spilling CA, Jones PW, Dodd JW, Barrick TR. White matter lesions characterise brain involvement in moderate to severe chronic obstructive pulmonary disease, but cerebral atrophy does not. *BMC Pulm Med.* 2017; 17. <https://doi.org/10.1186/s12890-017-0435-1> PMID: 28629404
12. Ryu CW, Jahng GH, Choi CW, Rhee HY, Kim M-J, Kim SM, et al. Microstructural change of the brain in chronic obstructive pulmonary disease. 2013; 10: 357–366.
13. Zhang H, Wang X, Lin J, Sun Y, Huang Y, Yang T, et al. Grey and white matter abnormalities in chronic obstructive pulmonary disease: a case-control study. *BMJ Open.* 2012; 2: e000844–e000844. <https://doi.org/10.1136/bmjopen-2012-000844> PMID: 22535793
14. Zeestraten EA, Lawrence AJ, Lambert C, Benjamin P, Brookes RL, Mackinnon AD, et al. Change in multimodal MRI markers predicts dementia risk in cerebral small vessel disease. *Neurology.* 2017; 89: 1869–1876. <https://doi.org/10.1212/WNL.0000000000004594> PMID: 28978655
15. Nave RD, Foresti S, Pratesi A, Ginestroni A, Inzitari M, Salvadori E, et al. Whole-Brain Histogram and Voxel-Based Analyses of Diffusion Tensor Imaging in Patients with Leukoaraiosis: Correlation with Motor and Cognitive Impairment. *Am J Neuroradiol.* 2007; 28: 1313–1319. <https://doi.org/10.3174/ajnr.A0555> PMID: 17698534
16. Nitkunan A, Charlton RA, McIntyre DJO, Barrick TR, Howe FA, Markus HS. Diffusion tensor imaging and MR spectroscopy in hypertension and presumed cerebral small vessel disease. *Magn Reson Med.* 2008; 59: 528–534. <https://doi.org/10.1002/mrm.21461> PMID: 18224697
17. Mesulam M-M. Large-scale neurocognitive networks and distributed processing for attention, language and memory. *Ann Neurol.* 1990; 28: 597–613. PMID: 2260847
18. Park H-J, Friston K. Structural and Functional Brain Networks: From Connections to Cognition. *Science.* 2013; 342: 1238411–1238411. <https://doi.org/10.1126/science.1238411> PMID: 24179229
19. Meunier D, Lambiotte R, Bullmore ET. Modular and Hierarchically Modular Organization of Brain Networks. *Front Neurosci.* 2010; 4. <https://doi.org/10.3389/fnins.2010.00200> PMID: 21151783
20. Bullmore E, Sporns O. The economy of brain network organization. *Nat Rev Neurosci.* 2012; <https://doi.org/10.1038/nrn3214> PMID: 22498897
21. Lawrence AJ, Chung AW, Morris RG, Markus HS, Barrick TR. Structural network efficiency is associated with cognitive impairment in small-vessel disease. *Neurology.* 2014; 83: 304–311. <https://doi.org/10.1212/WNL.0000000000000612> PMID: 24951477
22. Vogelmeier CF, Criner GJ, Martinez FJ, Anzueto A, Barnes PJ, Bourbeau J, et al. Global Strategy for the Diagnosis, Management, and Prevention of Chronic Obstructive Lung Disease 2017 Report. GOLD Executive Summary. *Am J Respir Crit Care Med.* 2017; 195: 557–582. <https://doi.org/10.1164/rccm.201701-0218PP> PMID: 28128970
23. Sabit R, Bolton CE, Edwards PH, Pettit RJ, Evans WD, McEniery CM, et al. Arterial stiffness and osteoporosis in chronic obstructive pulmonary disease. *Am J Respir Crit Care Med.* 2007; 175: 1259–1265. <https://doi.org/10.1164/rccm.200701-067OC> PMID: 17363772
24. D'Agostino R B. Stroke risk profile: adjustment for antihypertensive medication. The Framingham Study. *Stroke.* 1994; 25: 40–43. <https://doi.org/10.1161/01.str.25.1.40> PMID: 8266381
25. Charlson ME, Pompei P, Ales KL, MacKenzie CR. A new method of classifying prognostic comorbidity in longitudinal studies: development and validation. *J Chronic Dis.* 1987; 40: 373–383. [https://doi.org/10.1016/0021-9681\(87\)90171-8](https://doi.org/10.1016/0021-9681(87)90171-8) PMID: 3558716
26. Jones PW, Quirk FH, Baveystock CM, Littlejohns P. A self-complete measure of health status for chronic airflow limitation. The St. George's Respiratory Questionnaire. *Am Rev Respir Dis.* 1992; 145: 1321–1327. <https://doi.org/10.1164/ajrccm/145.6.1321> PMID: 1595997
27. Zigmund AS, Snaith RP. The hospital anxiety and depression scale. *Acta Psychiatr Scand.* 1983; 67: 361–370. <https://doi.org/10.1111/j.1600-0447.1983.tb09716.x> PMID: 6880820
28. Jenkinson M, Beckmann CF, Behrens TEJ, Woolrich MW, Smith SM. FSL. *NeuroImage.* 2012; 62: 782–790. <https://doi.org/10.1016/j.neuroimage.2011.09.015> PMID: 21979382

29. Smith SM. Fast robust automated brain extraction. *Hum Brain Mapp.* 2002; 17: 143–155. <https://doi.org/10.1002/hbm.10062> PMID: 12391568
30. Lambert C, Sam Narean J, Benjamin P, Zeestraten E, Barrick TR, Markus HS. Characterising the grey matter correlates of leukoaraiosis in cerebral small vessel disease. *NeuroImage Clin.* 2015; 9: 194–205. <https://doi.org/10.1016/j.nicl.2015.07.002> PMID: 26448913
31. Bullmore E, Sporns O. Complex brain networks: graph theoretical analysis of structural and functional systems. *Nat Rev Neurosci.* 2009; 10: 186–198. <https://doi.org/10.1038/nrn2575> PMID: 19190637
32. Tzourio-Mazoyer N, Landeau B, Papathanassiou D, Crivello F, Etard O, Delcroix N, et al. Automated Anatomical Labeling of Activations in SPM Using a Macroscopic Anatomical Parcellation of the MNI MRI Single-Subject Brain. *NeuroImage.* 2002; 15: 273–289. <https://doi.org/10.1006/nimg.2001.0978> PMID: 11771995
33. Greve DN, Fischl B. Accurate and robust brain image alignment using boundary-based registration. *NeuroImage.* 2009; 48: 63–72. <https://doi.org/10.1016/j.neuroimage.2009.06.060> PMID: 19573611
34. Holmes CJ, Hoge R, Collins L, Woods R, Toga AW, Evans AC. Enhancement of MR images using registration for signal averaging. *J Comput Assist Tomogr.* 1998; 22: 324–333. <https://doi.org/10.1097/00004728-199803000-00032> PMID: 9530404
35. Avants BB, Tustison NJ, Song G, Cook PA, Klein A, Gee JC. A reproducible evaluation of ANTs similarity metric performance in brain image registration. *NeuroImage.* 2011; 54: 2033–2044. <https://doi.org/10.1016/j.neuroimage.2010.09.025> PMID: 20851191
36. Calamante F, Tournier J-D, Jackson GD, Connelly A. Track-density imaging (TDI): super-resolution white matter imaging using whole-brain track-density mapping. *NeuroImage.* 2010; 53: 1233–1243. <https://doi.org/10.1016/j.neuroimage.2010.07.024> PMID: 20643215
37. Hagmann P, Kurlant M, Gigandet X, Thiran P, Wedeen VJ, Meuli R, et al. Mapping Human Whole-Brain Structural Networks with Diffusion MRI. Sporns O, editor. *PLoS ONE.* 2007; 2: e597. <https://doi.org/10.1371/journal.pone.0000597> PMID: 17611629
38. van den Heuvel MP, Sporns O. Rich-club organization of the human connectome. *J Neurosci Off J Soc Neurosci.* 2011; 31: 15775–15786. <https://doi.org/10.1523/JNEUROSCI.3539-11.2011> PMID: 22049421
39. Rubinov M, Sporns O. Complex network measures of brain connectivity: Uses and interpretations. *NeuroImage.* 2010; 52: 1059–1069. <https://doi.org/10.1016/j.neuroimage.2009.10.003> PMID: 19819337
40. Maslov S, Sneppen K. Specificity and stability in topology of protein networks. *Science.* 2002; 296: 910–913. <https://doi.org/10.1126/science.1065103> PMID: 11988575
41. Garrison KA, Scheinost D, Finn ES, Shen X, Constable RT. The (in)stability of functional brain network measures across thresholds. *NeuroImage.* 2015; 118: 651–661. <https://doi.org/10.1016/j.neuroimage.2015.05.046> PMID: 26021218
42. Ginestet CE, Fournel AP, Simmons A. Statistical network analysis for functional MRI: summary networks and group comparisons. *Front Comput Neurosci.* 2014; 8. <https://doi.org/10.3389/fncom.2014.00051> PMID: 24834049
43. Drakesmith M, Caeyenberghs K, Dutt A, Lewis G, David AS, Jones DK. Overcoming the effects of false positives and threshold bias in graph theoretical analyses of neuroimaging data. *NeuroImage.* 2015; 118: 313–333. <https://doi.org/10.1016/j.neuroimage.2015.05.011> PMID: 25982515
44. Drakesmith M, Caeyenberghs K, Dutt A, Zammit S, Evans CJ, Reichenberg A, et al. Schizophrenia-like topological changes in the structural connectome of individuals with subclinical psychotic experiences: Connectome Changes in Subclinical Psychosis. *Hum Brain Mapp.* 2015; 36: 2629–2643. <https://doi.org/10.1002/hbm.22796> PMID: 25832856
45. Bassett DS, Bullmore E. Small-world brain networks. *Neurosci Rev J Bringing Neurobiol Neurol Psychiatry.* 2006; 12: 512–523. <https://doi.org/10.1177/1073858406293182> PMID: 17079517
46. Zhang J, Wang Y, Wang J, Zhou X, Shu N, Wang Y, et al. White matter integrity disruptions associated with cognitive impairments in type 2 diabetes patients. *Diabetes.* 2014; DB_140342. <https://doi.org/10.2337/db14-0342> PMID: 24947353
47. van Duinkerken E, Schoonheim MM, IJzerman RG, Klein M, Ryan CM, Moll AC, et al. Diffusion tensor imaging in type 1 diabetes: decreased white matter integrity relates to cognitive functions. *Diabetologia.* 2012; 55: 1218–1220. <https://doi.org/10.1007/s00125-012-2488-2> PMID: 22327286
48. Kennedy KM, Raz N. Pattern of normal age-related regional differences in white matter microstructure is modified by vascular risk. *Brain Res.* 2009; 1297: 41–56. <https://doi.org/10.1016/j.brainres.2009.08.058> PMID: 19712671
49. Matsuda-Abenedini M, Fitzpatrick K, Harrell WR, Gipson DS, Hooper SR, Belger A, et al. Brain abnormalities in children and adolescents with chronic kidney disease. *Pediatr Res.* 2018; <https://doi.org/10.1038/s41390-018-0037-5> PMID: 29967532

50. Vemuri P, Knopman DS, Jack CR, Lundt ES, Weigand SD, Zuk SM, et al. Association of Kidney Function Biomarkers with Brain MRI Findings: The BRINK Study. *J Alzheimers Dis JAD*. 2017; 55: 1069–1082. <https://doi.org/10.3233/JAD-160834> PMID: 27767995
51. Wardlaw JM, Smith C, Dichgans M. Mechanisms of sporadic cerebral small vessel disease: insights from neuroimaging. *Lancet Neurol*. 2013; 12: 483–497. [https://doi.org/10.1016/S1474-4422\(13\)70060-7](https://doi.org/10.1016/S1474-4422(13)70060-7) PMID: 23602162
52. Li J, Fei G-H. The unique alterations of hippocampus and cognitive impairment in chronic obstructive pulmonary disease. *Respir Res*. 2013; 14: 1–9. <https://doi.org/10.1186/1465-9921-14-1>
53. Esser RW, Stoeckel MC, Kirsten A, Watz H, Taube K, Lehmann K, et al. Structural Brain Changes in Patients With COPD. *Chest*. 2016; 149: 426–434. <https://doi.org/10.1378/chest.15-0027> PMID: 26203911
54. Wang C, Ding Y, Shen B, Gao D, An J, Peng K, et al. Altered Gray Matter Volume in Stable Chronic Obstructive Pulmonary Disease with Subclinical Cognitive Impairment: an Exploratory Study. *Neurotox Res*. 2017; 31: 453–463. <https://doi.org/10.1007/s12640-016-9690-9> PMID: 28005183
55. Liao D, Higgins M, Bryan NR, Eigenbrodt ML, Chambless LE, Lamar V, et al. Lower pulmonary function and cerebral subclinical abnormalities detected by MRI: the Atherosclerosis Risk in Communities study. *Chest*. 1999; 116: 150–156. <https://doi.org/10.1378/chest.116.1.150> PMID: 10424519
56. Taki Y, Kinomura S, Ebihara S, Thyreau B, Sato K, Goto R, et al. Correlation between pulmonary function and brain volume in healthy elderly subjects. *Neuroradiology*. 2013; 55: 689–695. <https://doi.org/10.1007/s00234-013-1157-6> PMID: 23440433
57. Sachdev PS, Anstey KJ, Parslow RA, Wen W, Maller J, Kumar R, et al. Pulmonary Function, Cognitive Impairment and Brain Atrophy in a Middle-Aged Community Sample. *Dement Geriatr Cogn Disord*. 2006; 21: 300–308. <https://doi.org/10.1159/000091438> PMID: 16484809
58. Murray AD, Staff RT, Shenkin SD, Deary IJ, Starr JM, Whalley LJ. Brain white matter hyperintensities: relative importance of vascular risk factors in nondemented elderly people. *Radiology*. 2005; 237: 251–257. <https://doi.org/10.1148/radiol.2371041496> PMID: 16126931
59. van Dijk EJ, Prins ND, Vrooman HA, Hofman A, Koudstaal PJ, Breteler MMB. Progression of Cerebral Small Vessel Disease in Relation to Risk Factors and Cognitive Consequences: Rotterdam Scan Study. *Stroke*. 2008; 39: 2712–2719. <https://doi.org/10.1161/STROKEAHA.107.513176> PMID: 18635849
60. Debette S, Markus HS. The clinical importance of white matter hyperintensities on brain magnetic resonance imaging: systematic review and meta-analysis. *BMJ*. 2010; 341: c3666–c3666. <https://doi.org/10.1136/bmj.c3666> PMID: 20660506
61. Lucas P, Izquierdo JL, Gonzalez-Moro, Frances Fernandez, Lopez V, Cano Bellon. Chronic obstructive pulmonary disease as a cardiovascular risk factor. Results of a case–control study (CONSISTE study). *Int J Chron Obstruct Pulmon Dis*. 2012; 679. <https://doi.org/10.2147/COPD.S36222> PMID: 23055717
62. Lahousse L, Tiemeier H, Ikram MA, Brusselle GG. Chronic obstructive pulmonary disease and cerebrovascular disease: A comprehensive review. *Respir Med*. 2015; 109: 1371–1380. <https://doi.org/10.1016/j.rmed.2015.07.014> PMID: 26342840
63. Tuladhar AM, van Dijk E, Zwiers MP, van Norden AGW, de Laat KF, Shumskaya E, et al. Structural network connectivity and cognition in cerebral small vessel disease: Structural Network and Cognition. *Hum Brain Mapp*. 2016; 37: 300–310. <https://doi.org/10.1002/hbm.23032> PMID: 26466741
64. Wei R, Li C, Fogelson N, Li L. Prediction of Conversion from Mild Cognitive Impairment to Alzheimer's Disease Using MRI and Structural Network Features. *Front Aging Neurosci*. 2016; 8. <https://doi.org/10.3389/fnagi.2016.00076> PMID: 27148045
65. Eijlers AJC, van Geest Q, Dekker I, Steenwijk MD, Meijer KA, Hulst HE, et al. Predicting cognitive decline in multiple sclerosis: a 5-year follow-up study. *Brain*. 2018; 141: 2605–2618. <https://doi.org/10.1093/brain/awy202> PMID: 30169585
66. Zeestraten EA, Lawrence AJ, Lambert C, Benjamin P, Brookes RL, Mackinnon AD, et al. Change in multimodal MRI markers predicts dementia risk in cerebral small vessel disease. *Neurology*. 2017; 89: 1869–1876. <https://doi.org/10.1212/WNL.0000000000004594> PMID: 28978655
67. Lawrence AJ, Zeestraten EA, Benjamin P, Lambert CP, Morris RG, Barrick TR, et al. Longitudinal decline in structural networks predicts dementia in cerebral small vessel disease. *Neurology*. 2018; 90: e1898–e1910. <https://doi.org/10.1212/WNL.0000000000005551> PMID: 29695593
68. Berlot R, Metzler-Baddeley C, Ikram MA, Jones DK, O'Sullivan MJ. Global Efficiency of Structural Networks Mediates Cognitive Control in Mild Cognitive Impairment. *Front Aging Neurosci*. 2016; 8. <https://doi.org/10.3389/fnagi.2016.00292> PMID: 28018208
69. Du J, Wang Y, Zhi N, Geng J, Cao W, Yu L, et al. Structural brain network measures are superior to vascular burden scores in predicting early cognitive impairment in post stroke patients with small vessel disease. *NeuroImage Clin*. 2019; 22: 101712. <https://doi.org/10.1016/j.nicl.2019.101712> PMID: 30772684

70. Satz P. Brain reserve capacity on symptom onset after brain injury: A formulation and review of evidence for threshold theory. *Neuropsychology*. 1993; 7: 273–295. <https://doi.org/10.1037/0894-4105.7.3.273>
71. Stern Y. What is cognitive reserve? Theory and research application of the reserve concept. *J Int Neuropsychol Soc*. 2002; 8: 448–460. PMID: [11939702](https://pubmed.ncbi.nlm.nih.gov/11939702/)
72. Stern Y. Cognitive reserve☆. *Neuropsychologia*. 2009; 47: 2015–2028. <https://doi.org/10.1016/j.neuropsychologia.2009.03.004> PMID: [19467352](https://pubmed.ncbi.nlm.nih.gov/19467352/)
73. Lezak M D., Howieson D B., Loring D W. *Neuropsychological Assessment*, 4th Edn. 2004.
74. Wolf H, Julin P, Gertz H-J, Winblad B, Wahlund L-O. Intracranial volume in mild cognitive impairment, Alzheimer's disease and vascular dementia: evidence for brain reserve? *Int J Geriatr Psychiatry*. 2004; 19: 995–1007. <https://doi.org/10.1002/gps.1205> PMID: [15449362](https://pubmed.ncbi.nlm.nih.gov/15449362/)
75. Dodd JW, Getov SV, Jones PW. Cognitive function in COPD. *European Respiratory Journal*. 2010; 35: 913–922. <https://doi.org/10.1183/09031936.00125109> PMID: [20356988](https://pubmed.ncbi.nlm.nih.gov/20356988/)
76. Aras YG, Tuñç A, Güngen BD, Güngen AC, Aydemir Y, Demiyürek BE. The effects of depression, anxiety and sleep disturbances on cognitive impairment in patients with chronic obstructive pulmonary disease. *Cogn Neurodyn*. 2017; 11: 565–571. <https://doi.org/10.1007/s11571-017-9449-x> PMID: [29147148](https://pubmed.ncbi.nlm.nih.gov/29147148/)
77. Omachi TA, Blanc PD, Claman DM, Chen H, Yelin EH, Julian L, et al. Disturbed Sleep among COPD Patients is Longitudinally Associated with Mortality and Adverse COPD Outcomes. *Sleep Med*. 2012; 13: 476–483. <https://doi.org/10.1016/j.sleep.2011.12.007> PMID: [22429651](https://pubmed.ncbi.nlm.nih.gov/22429651/)
78. Dag E, Bulcun E, Turkel Y, Ekici A, Ekici M. Factors Influencing Cognitive Function in Subjects With COPD. *Respiratory Care*. 2016; 61: 1044–1050. <https://doi.org/10.4187/respcare.04403> PMID: [26932385](https://pubmed.ncbi.nlm.nih.gov/26932385/)
79. Emery CF, Shermer RL, Hauck ER, Hsiao ET, MacIntyre NR. Cognitive and psychological outcomes of exercise in a 1-year follow-up study of patients with chronic obstructive pulmonary disease. *Health Psychol*. 2003; 22: 598–604. <https://doi.org/10.1037/0278-6133.22.6.598> PMID: [14640857](https://pubmed.ncbi.nlm.nih.gov/14640857/)
80. Xie X, Shi Y, Zhang J. Structural network connectivity impairment and depressive symptoms in cerebral small vessel disease. *J Affect Disord*. 2017; 220: 8–14. <https://doi.org/10.1016/j.jad.2017.05.039> PMID: [28575716](https://pubmed.ncbi.nlm.nih.gov/28575716/)
81. Lin F, Wu G, Zhu L, Lei H. Heavy smokers show abnormal microstructural integrity in the anterior corpus callosum: A diffusion tensor imaging study with tract-based spatial statistics. *Drug Alcohol Depend*. 2013; 129: 82–87. <https://doi.org/10.1016/j.drugalcdep.2012.09.013> PMID: [23062873](https://pubmed.ncbi.nlm.nih.gov/23062873/)
82. Lin L, Xue Y, Duan Q, Sun B, Lin H, Chen X, et al. Microstructural White Matter Abnormalities and Cognitive Dysfunction in Subcortical Ischemic Vascular Disease: an Atlas-Based Diffusion Tensor Analysis Study. *J Mol Neurosci MN*. 2015; 56: 363–370. <https://doi.org/10.1007/s12031-015-0550-5> PMID: [25859933](https://pubmed.ncbi.nlm.nih.gov/25859933/)
83. Zhang H, Wang X, Lin J, Sun Y, Huang Y, Yang T, et al. Reduced regional gray matter volume in patients with chronic obstructive pulmonary disease: a voxel-based morphometry study. *Am J Neuroradiol*. 2013; 34: 334–339. <https://doi.org/10.3174/ajnr.A3235> PMID: [22859277](https://pubmed.ncbi.nlm.nih.gov/22859277/)
84. Heinen R, Vlegels N, de Bresser J, Leemans A, Biessels GJ, Reijmer YD. The cumulative effect of small vessel disease lesions is reflected in structural brain networks of memory clinic patients. *NeuroImage Clin*. 2018; 19: 963–969. <https://doi.org/10.1016/j.nicl.2018.06.025> PMID: [30003033](https://pubmed.ncbi.nlm.nih.gov/30003033/)
85. Ciccarelli O, Parker GJM, Toosy AT, Wheeler-Kingshott C a. M, Barker GJ, Boulby PA, et al. From diffusion tractography to quantitative white matter tract measures: a reproducibility study. *NeuroImage*. 2003; 18: 348–359. PMID: [12595188](https://pubmed.ncbi.nlm.nih.gov/12595188/)
86. Behrens TEJ, Berg HJ, Jbabdi S, Rushworth MFS, Woolrich MW. Probabilistic diffusion tractography with multiple fibre orientations: What can we gain? *NeuroImage*. 2007; 34: 144–155. <https://doi.org/10.1016/j.neuroimage.2006.09.018> PMID: [17070705](https://pubmed.ncbi.nlm.nih.gov/17070705/)
87. Metzler-Baddeley C, O'Sullivan MJ, Bells S, Pasternak O, Jones DK. How and how not to correct for CSF-contamination in diffusion MRI. *NeuroImage*. 2012; 59: 1394–1403. <https://doi.org/10.1016/j.neuroimage.2011.08.043> PMID: [21924365](https://pubmed.ncbi.nlm.nih.gov/21924365/)
88. Berlot R, Metzler-Baddeley C, Jones DK, O'Sullivan MJ. CSF contamination contributes to apparent microstructural alterations in mild cognitive impairment. *NeuroImage*. 2014; 92: 27–35. <https://doi.org/10.1016/j.neuroimage.2014.01.031> PMID: [24503415](https://pubmed.ncbi.nlm.nih.gov/24503415/)
89. Côté M-A, Girard G, Boré A, Garyfallidis E, Houde J-C, Descoteaux M. Tractometer: towards validation of tractography pipelines. *Med Image Anal*. 2013; 17: 844–857. <https://doi.org/10.1016/j.media.2013.03.009> PMID: [23706753](https://pubmed.ncbi.nlm.nih.gov/23706753/)
90. Tournier J-D, Calamante F, Gadian DG, Connelly A. Direct estimation of the fiber orientation density function from diffusion-weighted MRI data using spherical deconvolution. *NeuroImage*. 2004; 23: 1176–1185. <https://doi.org/10.1016/j.neuroimage.2004.07.037> PMID: [15528117](https://pubmed.ncbi.nlm.nih.gov/15528117/)

91. Tournier J-D, Calamante F, Connelly A. Robust determination of the fibre orientation distribution in diffusion MRI: non-negativity constrained super-resolved spherical deconvolution. *NeuroImage*. 2007; 35: 1459–1472. <https://doi.org/10.1016/j.neuroimage.2007.02.016> PMID: 17379540
92. Farquharson S, Tournier J-D, Calamante F, Fabinyi G, Schneider-Kolsky M, Jackson GD, et al. White matter fiber tractography: why we need to move beyond DTI. *J Neurosurg*. 2013; 118: 1367–1377. <https://doi.org/10.3171/2013.2.JNS121294> PMID: 23540269